

Broadband gradient index microwave quasi-optical elements based on non-resonant metamaterials

Ruopeng Liu,¹ Qiang Cheng,² Jessie Y. Chin,²
Jack J. Mock,¹ Tie Jun Cui,² and David R. Smith^{1,*}

¹Center for Metamaterials and Integrated Plasmonics and Department of Electrical and Computer Engineering,
Duke University, Box 90291, Durham, NC 27708, USA

²The State Key Laboratory of Millimeter Waves, Department of Radio Engineering, Southeast University, Nanjing
210096, P. R. China

*drsmith@ee.duke.edu

Abstract: Utilizing non-resonant metamaterial elements, we demonstrate that complex gradient index optics can be constructed exhibiting low material losses and large frequency bandwidth. Although the range of structures is limited to those having only electric response, with an electric permittivity always equal to or greater than unity, there are still numerous metamaterial design possibilities enabled by leveraging the non-resonant elements. For example, a gradient, impedance matching layer can be added that drastically reduces the return loss of the optical elements due to reflection. In microwave experiments, we demonstrate the broadband design concepts with a gradient index lens and a beam-steering element, both of which are confirmed to operate over the entire X-band (roughly 8-12 GHz) frequency spectrum.

©2009 Optical Society of America

OCIS codes: (160.3918) Materials; (220.3630) Optical Design and Fabrication; (260.2110) Physics Optics; (080.2710) Geometric Optics;

References and links

1. R. A. Shelby, D. R. Smith, and S. Schultz, "Experimental Verification of a Negative Index of Refraction," *Science* **292**(5514), 77–79 (2002).
2. J. B. Pendry, A. J. Holden, D. J. Robbins, and W. J. Stewart, "Magnetism from Conductors and Enhanced Non-Linear Phenomena," *IEEE Trans. Microw. Theory Tech.* **47**(11), 2075–2084 (1999).
3. W. E. Kock, "Metallic delay lenses," *Bell Syst. Tech. J.* **27**, 58 (1948).
4. R. W. Corkum, "isotropic artificial dielectric," *Proceedings of the IRE* **40**(5), 574–587 (1952).
5. J. Brown, and W. Jackson, "The Properties of Artificial Dielectrics at Centimetre Wavelengths," *Proc. IEE paper no.1699R vol. 102B pp. 11–21, January 1995.*
6. I. Bahl, and K. Gupta, "A leaky-wave antenna using an artificial dielectric medium," *IEEE Trans. Antenn. Propag.* **22**(1), 119–122 (1974).
7. Y. Mukoh, T. Nojima, and N. Hasebe, "A reflector lens antenna consisting of an artificial dielectric," *Electronics and Communications in Japan* **(1)**, 82 (1999).
8. I. Awai, H. Kubo, T. Iribe, D. Wakamiya, and A. Sanada, "An artificial dielectric material of huge permittivity with novel anisotropy and its application to a microwave BPF," in *Microwave Symposium Digest, 2003 IEEE MTT-S International* **2** 1085–1088 (2003).
9. I. Awai, S. Kida, and O. Mizue, "Very Thin and Flat Lens Antenna Made of Artificial Dielectrics," in *2007 Korea-Japan Microwave Conference* 177–180 (2007).
10. I. Awai, "Artificial Dielectric Resonators for Miniaturized Filters," *IEEE Microw. Mag.* **9**(5), 55–64 (2008).
11. Y. Ma, B. Rejaei, and Y. Zhuang, "Radial Perfectly Matched Layer for the ADI-FDTD Method," *IEEE Microw. Wirel. Compon. Lett.* **19**, 431–433 (2008).
12. J. B. Pendry, D. Schurig, and D. R. Smith, "Controlling electromagnetic fields," *Science* **312**(5781), 1780–1782 (2006).
13. J. B. Pendry, and S. A. Ramakrishna, "Focusing light with negative refractive index," *J. Phys. Condens. Matter* **15**(37), 6345–6364 (2003).
14. S. Guenneau, B. Gralak, and J. B. Pendry, "Perfect corner reflector," *Opt. Lett.* **30**(10), 1204–1206 (2005).

15. D. Schurig, J. J. Mock, B. J. Justice, S. A. Cummer, J. B. Pendry, A. F. Starr, and D. R. Smith, "Metamaterial electromagnetic cloak at microwave frequencies," *Science* **314**(5801), 977–980 (2006).
 16. R. Liu, T. J. Cui, D. Huang, B. Zhao, and D. R. Smith, "Description and explanation of electromagnetic behaviors in artificial metamaterials based on effective medium theory," *Phys. Rev. E Stat. Nonlin. Soft Matter Phys.* **76**(2), 026606 (2007).
 17. C. Kittel, *Solid State Physics* (John Wiley & Sons, New York, 1986), 6th ed., p275.
 18. G. Dolling, C. Enkrich, and M. Wegener, S. Linden, J. Zhou, and C. M. Soukoulis, "Cut-wire and plate capacitors as magnetic atoms for optical metamaterials," *Opt. Lett.* **30**, 3198 (2005).
 19. D. R. Smith, P. M. Rye, J. J. Mock, D. C. Vier, and A. F. Starr, "Enhanced diffraction from a grating on the surface of a negative-index metamaterial," *Phys. Rev. Lett.* **93**(13), 137405 (2004).
 20. M. J. Minot, "Single-layer, gradient refractive index antireflection films effective from 0.35 μm to 2.5 μm ," *J. Opt. Soc. Am.* **66**(6), 515–519 (1976).
 21. R. Jacobson, "Inhomogeneous and coevaporated homogeneous films for optical applications," in *Physics of Thin Films*, G. Haas, M. Francombe, and R. Hoffman, eds. (Academic, New York, 1975), Vol. 8, p. 51.
 22. C. G. Snedaker, "New numerical thin-film synthesis technique," *J. Opt. Soc. Am.* **72**, 1732 (1982).
 23. B. J. Justice, J. J. Mock, L. Guo, A. Degiron, D. Schurig, and D. R. Smith, "Spatial mapping of the internal and external electromagnetic fields of negative index metamaterials," *Opt. Express* **14**(19), 8694–8705 (2006).
 24. J. Li, and J. B. Pendry, "Hiding under the Carpet: a New Strategy for Cloaking," *Phys. Rev. Lett.* **101**(20), 203901 (2008).
 25. R. Liu, C. Ji, J. J. Mock, J. Y. Chin, T. J. Cui, and D. R. Smith, "Broadband ground-plane cloak," *Science* **323**(5912), 366–369 (2009).
-

1. Introduction

Because the electromagnetic response of metamaterial elements can be precisely controlled, they can be utilized as the fundamental building blocks for a wide range of complex, electromagnetic media. The sub-wavelength, resonant, conducting circuits frequently used to form the underlying structure of metamaterials are capable of producing a wide range of exotic material response. Given the design flexibility inherent to resonant elements, metamaterials have been constructed with electromagnetic properties difficult or impossible to achieve using conventional materials. A surge of interest, for example, was sparked after the demonstration of a left-handed metamaterial, since the negative index-of-refraction associated with such materials is not a property available in nature [1]. Artificial magnetism is another example of a material property that can be achieved through the use of resonant metamaterials and which can be scaled to wavelengths where magnetism is all but absent [2].

Though the field of metamaterials has developed rapidly over the last decade, the underlying effective medium concepts have been around for quite some time. The idea of mimicking the polarization response of atomic or molecular systems to form artificial dielectrics was proposed early on as a means of constructing lenses and other quasi-optical elements for microwave and millimeter wave devices [3–11]. Because the earlier analysis of artificial dielectrics was based on analytical methods, however, a convenient design methodology for highly complex, artificial media was not readily available.

More recently, metamaterials have become widely appreciated as a means of producing inhomogeneous media, in which the material properties vary in a controlled manner throughout space. Indeed, gradient index quasi-optical metamaterial devices have been demonstrated at microwave frequencies in several experiments. Moreover, since metamaterials allow unprecedented freedom to control the constitutive tensor elements independently, point-by-point throughout a region of space, they can be used as the technology to realize structures designed by the method of transformation optics [12–14]. The "invisibility" cloak, demonstrated at microwave frequencies in 2006, is an example of a metamaterial that achieves a transformation optical design [15]. Although metamaterials have proven successful in the realization of unusual electromagnetic response, the structures demonstrated are often of marginal utility in practical applications due to the large losses that are inherent to the resonant elements typically used.

2. Non-resonant metamaterial elements

In concept, non-resonant metamaterials can be obtained from simple, polarizable, conducting elements such as the one shown in the inset to Fig. 1. At some frequency there will occur an electric resonance due to the inductance of the length of conductor combined with the capacitance occurring between the elements. If a numerical retrieval is performed on the unit cell shown, the frequency dependent effective permittivity and permeability, shown in Fig. 1(a) and Fig. 1(b), are found. To obtain the effective constitutive parameters, we first perform a full-wave simulation to determine the exact local field distributions and scattering (S-) parameters. The simulations are carried out using HFSS (Ansoft), a commercial electromagnetic, finite-element, solver. The effective constitutive parameters are then obtained using a well-established retrieval method in which the simulated S-parameters from a single unit cell are inverted to find the effective permittivity and permeability that would describe the scattering of an equivalent length of homogeneous material.

Although the retrieved permittivity would be expected to exhibit a simple Lorentzian resonance and no magnetic response, the actual curves appear distorted and more complex. The additional features in the line shapes occur due to the effects of spatial dispersion. As described in Ref [16], the retrieved curves can be well described using the following approximate formulas

$$\begin{aligned}\epsilon_{eff} &= \bar{\epsilon}(f) \frac{(\theta/2)}{\sin(\theta/2)\cos(\theta/2)} \\ \mu_{eff} &= \bar{\mu}(f) \frac{\cos(\theta/2)}{\sin(\theta/2)} (\theta/2)\end{aligned}\tag{1}$$

in which, $\theta = 2\pi fp\sqrt{\epsilon\mu}$, $f = \omega/2\pi$ and p is the periodicity of the unit cell. Equation (1) shows that the observed line shape for the permittivity, $\epsilon_{eff}(f)$, is the product of the averaged permittivity multiplied by a factor accounting for the spatial dispersion.

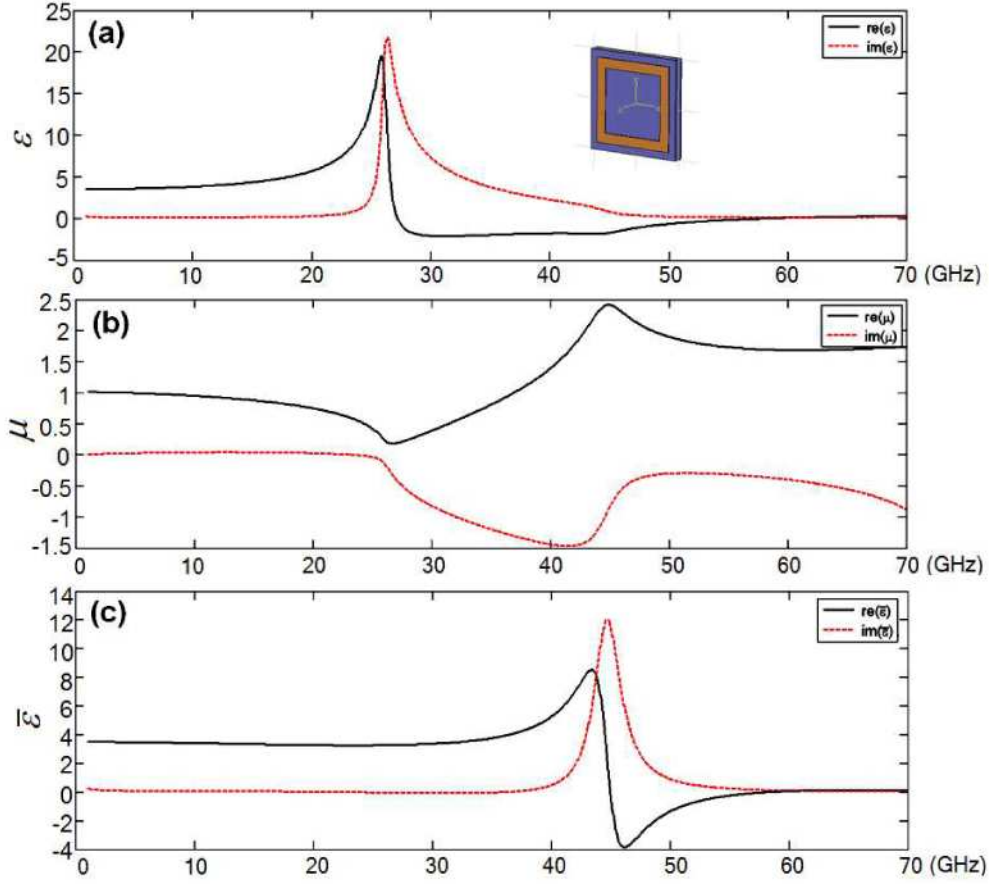


Fig. 1. (a) Retrieved permittivity for a metamaterial composed of the repeated unit cell shown in the inset; (b) retrieved permeability for a metamaterial composed of the repeated unit cell shown in the inset. (c) The distortions and artifacts in the retrieved parameters are due to spatial dispersion, which can be removed to find the Drude-Lorentz like resonance shown in the lower figure.

Figure 1(c) shows $\bar{\epsilon}$ as a function of frequency, revealing a regular Drude-Lorentz resonant form. The element possesses a resonance in the permittivity at a frequency near 42 GHz. The observed electric resonance has the form

$$\epsilon(\omega) = 1 - \frac{f_p^2}{f^2 - f_0^2 + i\Gamma f} = \frac{f^2 - f_0^2 - f_p^2 - i\Gamma f}{f^2 - f_0^2 + i\Gamma f} \quad (2)$$

where f_p is the plasma frequency, f_0 is the resonance frequency and Γ is a damping factor. Neglecting loss, the frequency where $\epsilon(f) = 0$ occurs at $f_L^2 = f_0^2 + f_p^2$. In the zero frequency limit we find

$$\epsilon(\omega \rightarrow 0) = 1 + \frac{f_p^2}{f_0^2} = \frac{f_L^2}{f_0^2} \quad (3)$$

an equation reminiscent of the Lyddane-Sachs-Teller relation that describes the contribution of the polariton resonance to the dielectric constant at zero frequency [17]. At frequencies far away from the resonance, we see that the permittivity approaches a constant that differs from

unity by the square of the ratio of the plasma to the resonance frequencies. Although the values of the permittivity are necessarily positive and greater than unity, the permittivity is nearly dispersionless and lossless—a considerable advantage. Note that this property does not extend to magnetic metamaterial media, such as split ring resonators, which are generally characterized by effective permeability of the form

$$\mu(f) = 1 - \frac{Ff^2}{f^2 - f_0^2 + i\Gamma f} \quad (4)$$

which approaches unity in the low frequency limit. Because artificial magnetic effects are based on induction rather than polarization, artificial magnetic response must vanish at zero frequency.

3. Broadband metamaterial device design

The general approach to the design of an artificial dielectrics, then, is to alter the geometry of an electric metamaterial element so that the effective plasma frequency and resonance frequency are altered according to Eq. (2). At frequencies well below the resonance, the unit cell behaves as an effective medium, with an effective permittivity that exhibits low loss and low dispersion. The value of the permittivity is given approximately by Eq. (3).

The closed ring element, shown in Fig. (1), is a simple geometry that can be utilized as the basic unit for a variety of electric metamaterials. The response of the closed ring structure is identical to the “cut-wire” structure previously studied [18], where it has been shown that the plasma and resonance frequencies are simply related to circuit parameters according to $\omega_p^2 \approx 1/L$ and $\omega_0^2 \approx 1/(LC)$. Here, L is the inductance associated with the arms of the closed ring and C is the capacitance associated with the gap between adjacent closed rings. For a fixed unit cell size, the inductance can be tuned either by changing the thickness, w , of the conducting rings or their length, a . The capacitance can be controlled primarily by changing the overall size of the ring.

It should be noted that though the design procedure is straightforward in concept, the effects caused by spatial dispersion represent a complication that increases the need for accurate numerical simulations of the unit cell. Although the structure is of a certain of anisotropy and coupling along the propagation direction that is not considered in the retrieval process, we notice that the unit cell is much smaller than the wavelength and works far from the resonance, the coupling is not significant and the anisotropy will not affect refractive index much.

Changing the resonant circuit of the metamaterial element tunes the low frequency permittivity value, as illustrated by the simulation results presented in Fig. 2. The closed ring structure shown in Fig. 2(a) is assumed to be deposited on FR4 substrate, whose permittivity is $3.85 + 0.02i$ and whose thickness is 0.2026 mm. The unit cell is cubic with dimension 2 mm and the thickness of the deposited metal layer (assumed to be copper) is 0.018 mm. For this structure, a resonance occurs near 25 GHz with the permittivity nearly constant over a large frequency region (roughly zero to 15 GHz). Simulations of three different unit cells with ring dimensions of $a = 0.7$ mm, 1.4 mm and 1.625 mm (all other parameters held fixed) were also simulated to illustrate the effect on the material parameters. In Fig. 2b, it is observed that the index value becomes larger as the ring dimension is increased, reflecting the larger polarizability of the larger rings.

The refractive index remains, for the most part, relatively flat as a function of frequency for frequencies well below the resonance. The index does exhibit a slight monotonic increase as a function of frequency, however, as the higher frequency resonance is approached. The impedance also varies somewhat as a function of frequency due to the effects of spatial dispersion. The losses in this structure are found to be negligible, as a result of being far away from the resonance frequency. This result is especially striking, because the substrate is not

one optimized for RF circuits—in fact, the FR4 circuit board substrate assumed here is generally considered quite lossy at microwave frequencies.

To illustrate the utility of non-resonant metamaterial elements to facilitate complex media, we make use of the closed ring to form two gradient index (GRIN) devices: a gradient index lens and a gradient index beam steering. The design approach is first to determine the desired continuous index profile that accomplishes the desired function (e.g., focusing or steering) and then to stepwise approximate the index profile using a discrete number of metamaterial elements. The elements can be designed by performing numerical simulations for a large number of variations of the geometrical parameters of the unit cell (i.e., a , w , etc.); once enough simulations have been run so that a reasonable interpolation can be formed of the permittivity as a function of the geometrical parameters, the metamaterial gradient index structure can be laid out and fabricated. This basic approach has been followed in [19].

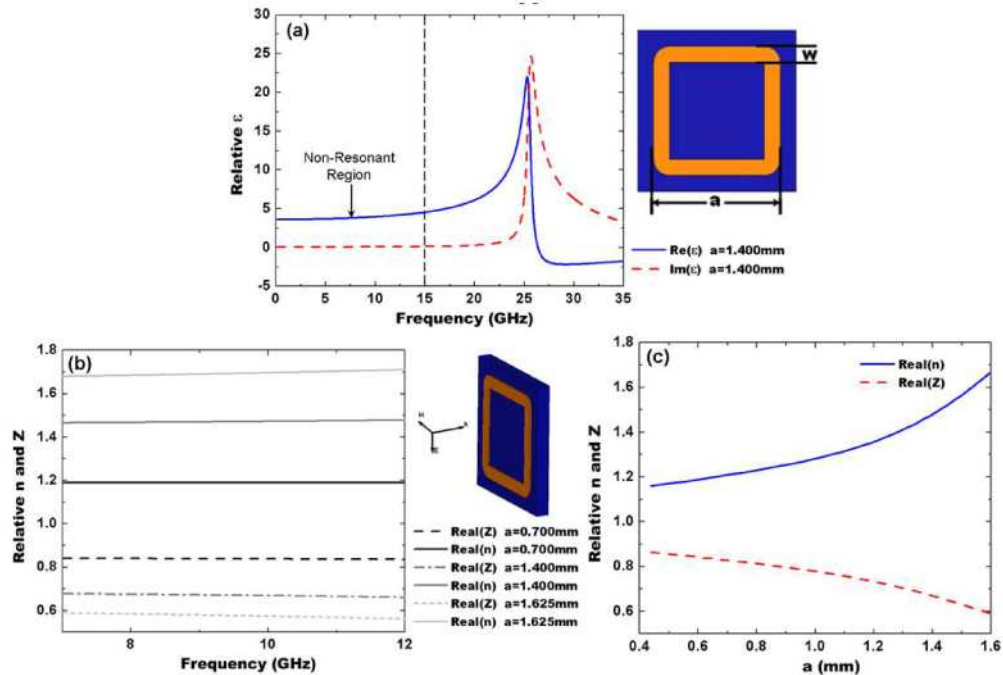


Fig. 2. Retrieval results for the closed ring medium. In all cases the radius of curvature of the corners is 0.6 mm, $w=0.2$ mm and unit cell periodicity is 2 mm. (a) The extracted permittivity with $a=1.4$ mm. (b) The extracted index and impedance for several values of a . The low frequency region is shown. (c) The relationship between the dimension a and the extracted refractive index and wave impedance.

The index distributions corresponding to two gradient index devices are shown in Fig. 3. Both devices are composed of three functional gradient layers. The middle layer performs the main function of the device, whether steering (Fig. 3(a)) or focusing (Fig. 3(b)) electromagnetic waves. The input and output layers are impedance matching layers (IMLs) that effectively match the impedance of the GRIN device to free space, reducing the reflected power and minimizing the overall insertion loss. Although the index (and thus the impedance) of either device varies across its length, we assume an input beam with Gaussian profile will be incident on the central region. Thus, the IMLs are designed to step the index from free space values to the index at the center of the GRIN region.

It should be noted that the gradients used to form the IML are quite different in spirit from those used to implement the focusing or steering functionality. There is a rapid change in the refractive index (or impedance) across the IML, the length of which is smaller than the

wavelengths of operation. As such, the IML more closely resembles an impedance matching network whose layers can be optimized to achieve reduced reflectance over broad ranges of frequencies and incident angles [20–22].

To illustrate the function of the IML, we study the reflection coefficient between air and a dielectric with refractive index $n=1.68$. Each metamaterial unit cell layer is modeled as a homogeneous dielectric with value of permittivity corresponding to that obtained by the unit cell retrievals. In Fig. 4(a), a metamaterial IML is shown composed of five layers, in which the index grades linearly from unity to $n=1.68$. The thickness of each layer is 2 mm. Here, the IML serves to match air to the higher dielectric half-space. Figure 4(b) shows a finite length of dielectric slab, on either side of which is placed IML layers. In this configuration, the dielectric slab is effectively matched to the lower dielectric space in which it is embedded. The reflectance (square of the reflection coefficient) as a function of frequency is shown for the half-space (Fig. 4(a)) and finite slab (Fig. 4(b)) in Fig. 4(c) and 4(d), respectively. In both cases, the reflectance is shown with and without the IML for comparison.

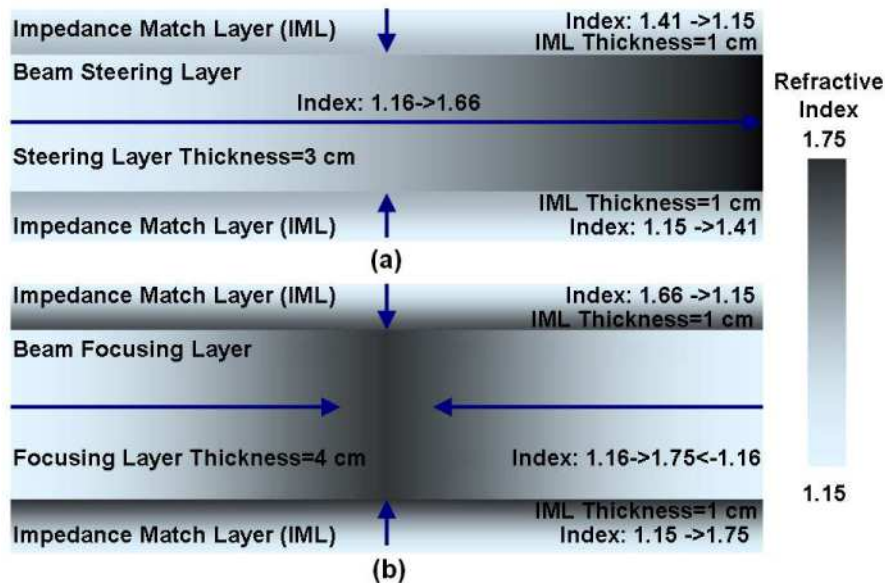


Fig. 3. Refractive index distributions for the designed gradient index structures. (a) A beam-steering element based on a linear index gradient. (b) A beam focusing lens, based on a higher order polynomial index gradient. Note the presence in both designs of an impedance matching layer (IML), provided to improve the insertion loss of the structures.

At very low frequencies, the wavelength becomes significantly larger than the IML length, and it can be expected that any gradient will become unimportant; we thus expect the reflectance to approach that given by the impedance mismatch between the half-space (or slab) and air. Figure 4(c) confirms that the reflectances for the IML and the control cases become identical as the frequency approaches zero. However, the reflectance drops quickly as the frequency is increased. At 5GHz, the reflectance has been reduced from 0.13 to below 0.04. Figure 4(d) illustrates the improvement in the reflectance achieved by adding IMLs to both interfaces of a dielectric slab. Again, a significant reduction in the overall reflectance is achieved, with the accompanying reduction in the Fabry-Perot type oscillations resulting from the dielectric slab acting as a cavity. This set of simulations illustrates the use of metamaterials to achieve controlled impedance matching. Note that neither in these illustrative calculations, nor in the experimentally fabricated structures shown in the next section, have we made any attempt to optimize the IMLs.

The two quasi-optical devices were first designed assuming continuous index profiles as in Fig. 3. The beam steering device is a slab with a linear index gradient in the direction transverse to the direction of wave propagation. The index values range from $n = 1.16$ to $n = 1.66$, consistent with the range available from the designed set of closed ring metamaterial elements obtained by varying the parameter a . An IML five unit cells in length is placed on both sides of the sample (input and output) with index values that change from unity (air) to $n = 1.41$, the index value at the center of the beam steering slab. This index value was chosen because most of the energy of the collimated beam passes through the center of the sample. To implement the actual beam steering sample, we made use of the closed ring unit cell shown in Fig. 2 and designed an array of unit cells having the distribution shown in Fig. 3(a).

The beam focusing lens is a planar slab with the index distribution as represented in Fig. 3(b). The index distribution has the functional form of

$$\text{Re}(n) = 4 \times 10^{-6} |x|^3 - 5 \times 10^{-4} |x|^2 - 6 \times 10^{-4} |x| + 1.75 \quad (5)$$

in which x is the distance away from the center of the lens. Once again, an IML was used to match the sample to free space. In this case, the index profile in the IML was ramped linearly from $n = 1.15$ to $n = 1.75$, the latter value selected to match the index at the center of the lens. Again, the IML layer was five unit cells in length. The same set of unit cell designs was utilized to implement the beam focusing lens as was used for the beam steering lens.

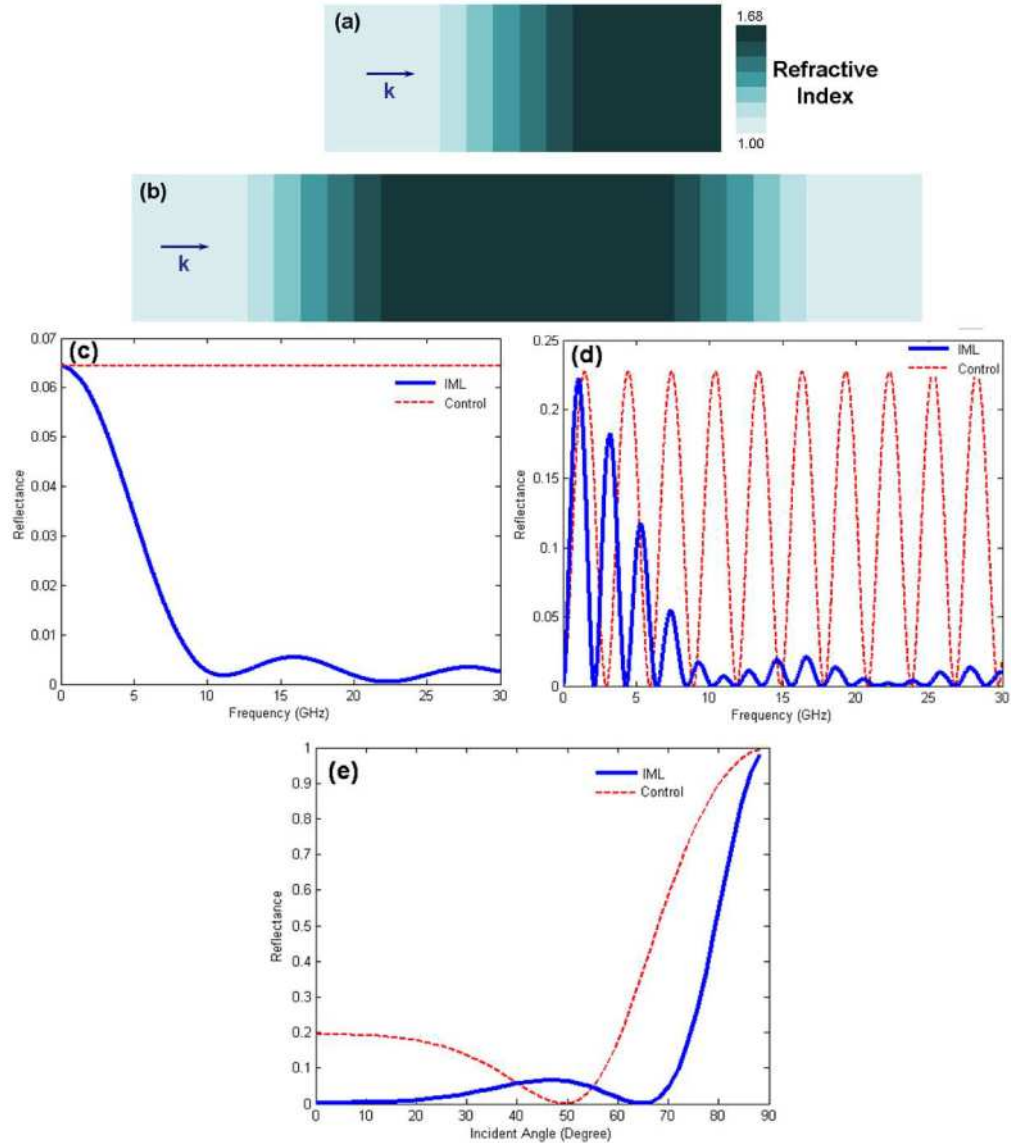


Fig. 4. Calculated reflected power of metamaterial impedance matching layers (IMLs) (a) An IML interface between air and a dielectric with refractive index $n=1.68$. (b) A dielectric slab ($n=1.68$) with two IML interfaces on either side, (c) Reflection calculation for a TEM wave for case (a) and its control without IML. (d) Reflection calculation on a TEM wave for case (b) and its control without IML. (e) Reflection calculation for an oblique incident TE wave. Note that the angle is measured with respect to the surface normal.

4. Experimental results

To confirm the properties of the gradient index structures, we fabricated the two designed samples, as examples, using copper clad FR4 printed circuit board substrate whose permittivity is $3.85+i0.02$, shown in Fig. 5. Following a procedure previously described [23], sheets of the samples were fabricated by standard optical lithography, then cut into 1 cm tall strips using a numerically controlled milling machine. The strips, held in place by unpatterned circuit board cross layers, were assembled together to form the gradient index slabs. For characterization, a 2D planar waveguide apparatus previously described was used [23]. The

planar waveguide supports transverse electric (TE) polarized waves, which are introduced into the waveguide via a coax-to-waveguide adapter. The incident waves are guided into the center of the chamber using tapered absorber that expands gradually from the output of the X-band waveguide adapter (2.29 cm) to a width of ~5-6 cm. The emerging beam, roughly Gaussian in profile, impinges directly on the GRIN samples. The characterization of the samples is accomplished by mapping the field distribution within and outside of the structures, using a coaxial cable inserted into the upper plate of the chamber. The lower plate is stepped in the lateral directions, such that a two dimensional image of the fields can be formed.

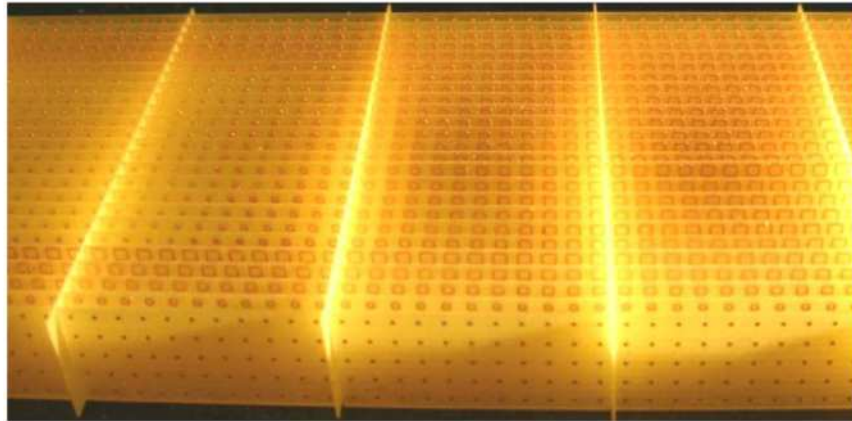


Fig. 5. Fabricated sample in which the design of each metamaterial element varies with the space coordinate.

The experimentally obtained electric field map associated with the beam steering structure is shown in Fig. 6. From the theoretical analysis in Fig. 2 and Fig. 4, the expected bandwidth spans the range from zero frequency to approximately 18GHz. Though we expect the GRIN structures to possess a very large effective bandwidth, the planar waveguide apparatus is configured to provide data only over the X-band frequency range (or ~7-13 GHz). To confirm the expected bandwidth, we acquired field mapping data over a number of frequencies throughout the X-band. Four field maps are shown in Fig. 6, corresponding to the frequencies 7.38 GHz, 8.5 GHz, 9.99 GHz and 11.72 GHz. In all cases, the beam was bent by a steering angle of 16.2 degrees, as indicated by the arrows in the plots in Fig. 6. Because the constituent metamaterial elements are used relatively far from their resonance frequencies, the energy loss of the beam as it propagates through the sample is extremely low and hardly observable from the measurements. The low insertion loss can be estimated by comparing the intensity of the color map corresponding to the wave at the entrance and the exit of the GRIN slab. Any loss of intensity observed in these data is more likely due to the effects of diffraction and the spreading of the beam rather than insertion losses.

The reflectance from the slab is also well-controlled by the IML; no significant standing waves can be observed in the field plots. Though the absence of standing waves is less apparent from the single image, it is possible to form a pseudo-animation of the data by advancing the phase from zero to 360 degrees. Because the complex fields are obtained via the network analyzer, the presence of standing waves would be noticeable as an oscillation in the intensity of the fields as a function of the phase advance. Instead, field animations reveal a nearly steady propagation behavior with very little oscillation in the overall intensity. The three layer GRIN slab thus smoothly compresses the incident wave into the higher index beam steering region with minimal reflection and with broad bandwidth.

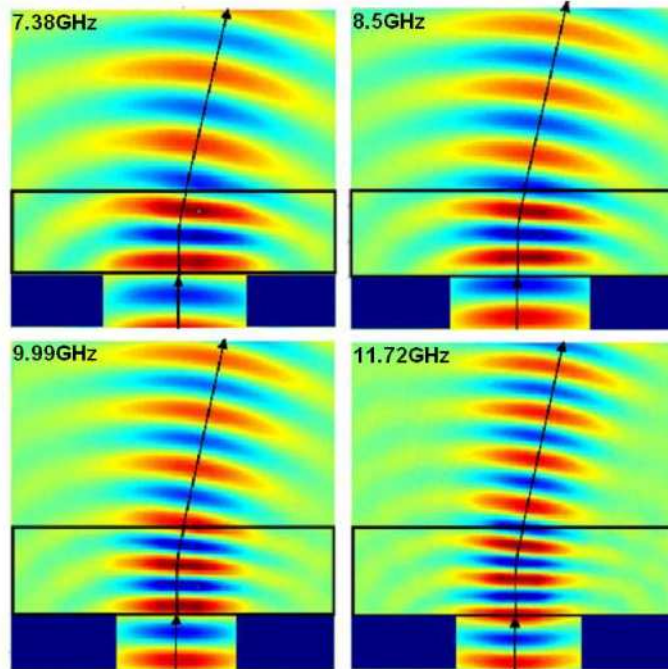


Fig. 6. Field mapping measurements of the beam steering lens. The lens has a linear gradient that causes the incoming beam to be deflected by an angle of 16.2 degrees. The effect is broadband, as can be seen from the identical maps taken at four different frequencies that span the X-band range of the experimental apparatus.

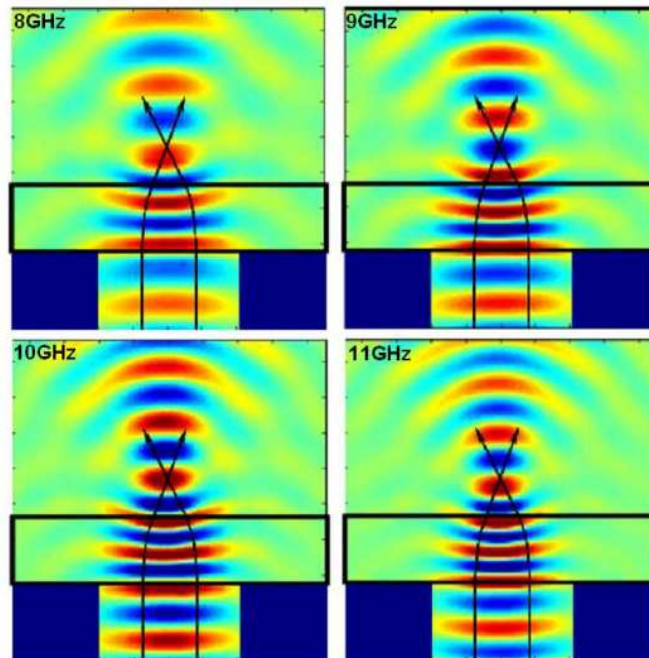


Fig. 7. Field mapping measurements of the beam focusing lens. The lens has a symmetric profile about the center (given in the text) that causes the incoming beam to be focused to a point. Once again, the function is broadband, as can be seen from the identical maps taken at four different frequencies that span the X-band range of the experimental apparatus.

The operation of the GRIN lens is illustrated in Fig. 7, which shows field maps taken at 8 GHz, 9 GHz, 10 GHz and 11 GHz. In all cases, a focal distance of 35 mm is observed with accompanying low insertion loss. The focusing properties of the lens were confirmed by introducing the same collimated beam at the sample input, which was brought to a focus on the exit side of the flat lens. The reflectance from the sample was again dramatically minimized by the IML design. The spatial distribution of the refractive index in the direction transverse to that of propagation in the middle layer serves to focus the wave. The arrows in Fig. 7 illustrate the wave vector and wave front of this short distance focus. Although not demonstrated here, the aberration of the focus can be further optimized by changing the refractive index distribution of IML and focusing functional layer, an aspect useful for quasi-optical components for antenna or communications applications.

Although these measurements confirm the broad band nature of the non-resonant metamaterial elements over the X-band range, we expect the actual bandwidth of the structures to be significantly larger, as indicated in the electromagnetic parameter retrieval analysis shown in in Fig. 1 and Fig. 2, virtually from zero frequency up to perhaps 18 GHz. The limit on the upper frequency is set by the position of the resonance of the elements, as well as the unit cell size relative to the wavelength of operation. While there is intrinsically no lower frequency limit on the non-resonant metamaterial element, the IML used to match the structures to free space has its own frequency dependent properties due to the gradient index design. From Fig. 4, we see that below 5 GHz the reflectance begins to rise substantially for the IML design employed. It should also be noted that the IML does not eliminate refractive effects at the interface, so that waves at oblique incidence on the IML interface will generally undergo a change in propagation direction. Though the effects of refraction are not so evident in the structures measured here, refractive effects could play a substantial role in other geometries.

We have demonstrated the use of non-resonant elements to form gradient index metamaterials with broad bandwidth and have illustrated the technique with specific designs of planar beam steering and focusing quasi-optical devices. Although we have illustrated the technique here with conventional devices, the capability of controlling the refractive index—or, more generally, the electric permittivity tensor components—throughout space can provide the means to form highly complex electromagnetic structures. This capability is of particular importance in the emerging field of transformation optics, where control of spatial gradients throughout a material is a critical, enabling step.

In a recent development, the concept of quasi-conformal transformations was introduced as a means of reducing the complexity of certain transformation optical designs [24]. Certain transformations can be constrained by the use of quasi-conformal methods to minimize the required magnetic response from the transformation optical medium. An index-only implementation of a transformation optical structure termed the “ground-plane cloak” was suggested by Li and Pendry, and subsequently demonstrated experimentally through the use of non-resonant metamaterials similar to those described in detail here [25]. The ability to form broad band, low loss, transformation optical media is a major advantage of non-resonant metamaterials. The same design rules can thus be applied to form both conventional and unconventional electromagnetic devices.

Acknowledgments

This work was supported by the Air Force Office of Scientific Research through a Multiple University Research Initiative, Contract No. FA9550-06-1-0279. The authors are grateful to Aloyse Degiron and Ekaterina Poutrina for helpful discussions and constructive comments.